Porous Silicon Antireflective Coatings for Silicon Solar Cells

Achoura-Mouna Mouafki
Department of Matter Sciences
Faculty of Exact Sciences and Sciences of Nature and Life
University Larbi Ben M'hidi
Oum El Bouaghi, Algeria
mouafki.mouna17@gmail.com

Faiza Bouaïcha
Laboratory of the Active Components and Materials
Institute of Science and Applied Techniques
University Larbi Ben M'hidi
Oum El Bouaghi, Algeria
f_bouaicha@yahoo.com

Abouelfath Hedibi
Materials Science and Informatics Laboratory
Faculty of Science
University of Djelfa
Djelfa, Algeria
abouelfath.hedibi@gmail.com

Ahmed Gueddim
Materials Science and Informatics Laboratory
Faculty of Science
University of Djelfa
Djelfa, Algeria
ahmed_gueddim@yahoo.fr

Received: 3 February 2022 | Revised: 11 February 2022 | Accepted: 13 February 2022

Abstract-This study presents a numerical investigation of the reflectivity of a Single Anti-Reflective Layer (SARL) and a stack of antireflective layers made of porous silicon. The stack consists of a certain number of periods, and each period contains two layers with different porosity. The simulations were conducted using the well-known Stratified Medium Theory (SMT) framework and the effect of porosity was studied. The optimal value was determined at 60% for the SARL and 65/55% for the stack of 12 periods and 6 layers. The angle of incidence was found to have more influence on the stack reflection than on the SARL reflection. The results of this investigation show that porous silicon can be used as an effective anti-reflective coating for silicon solar cells.

Keywords-porous silicon; silicon; solar cell;reflectivity

I. INTRODUCTION

The photovoltaic effect is defined as the direct transformation of electromagnetic energy (solar radiation) into directly usable continuous electrical energy, and it was discovered in 1839 [1]. The photovoltaic effect has been exploited for the design of photovoltaic solar cells. Since the 1990s, photovoltaic energy has attracted growing interest and many technological advances have been made through several technological sectors. Photovoltaic electricity production has increased exponentially since 2001, and projections are quite optimistic for the coming years [2]. Cell efficiency will certainly increase and, according to the Community Research and Development Information Service (CORDIS), the lifespan of cells in 2030 will be 40 years with an energy payback time of only one year and very satisfactory efficiency [3]. The efficiency of a solar cell is mainly limited by the various losses that occur in the cell. Among these losses, the reflection of incident photons at the surface of the cell (emitter, or window layer) contributes to the degradation of the collection efficiency of the cell. To remedy this problem, antireflection layers are often used on the front face of the cell to reduce the reflected fraction of incident radiation and improve the transport of carriers via the passivation of defects inside the cell [4-6]. The simplest way to create an anti-reflective coating is to deposit a quarter-wave layer of a dielectric with an intermediate refractive index between that of the emitter (or the window) and the air (TiO_2, Si_3N_4, Ta_2O_5, etc). For silicon, for example, a layer of Si_3N_4 quarter wavelength centered on the maximum of the solar spectrum AM1.5 reduces the reflection by 12% on average in the wavelength range 400-1100nm, increasing the photocurrent by 45% [7]. It should be noted that the reflection of silicon is between 35-40%, depending on the synthesis process [7-10]. In addition, porous silicon can be used as an alternative antireflective coating for silicon solar cells since the basis material is the same.

Porous silicon was accidentally discovered in the 1950s in an attempt to develop an electrochemical method to fabricate silicon substrates for microelectronic devices. Under the appropriate electrochemical conditions, the silicon substrate did not dissolve uniformly as expected. However, fine holes appeared, propagating primarily within the material in the [100] direction. Since this did not provide the desired smooth polish, the material was somewhat abandoned. During the 1970s and 1980s, significant interest arose because the high surface area of porous silicon was found to be useful as a model of the crystalline silicon surface in spectroscopic studies [11-14], as a precursor to generate thick oxide layers on silicon, and as a dielectric layer in capacitance-based chemical sensors [15]. Interest in porous silicon, and in particular its

Corresponding author: Achoura-Mouna Mouafki

nanostructure, exploded in the early 1990s when Ulrich Goesele at Duke University identified quantum confinement effects in the absorption spectrum of porous silicon, and almost simultaneously Leigh Canham in England reported efficient bright red-orange photoluminescence from the material [16, 17]. The quantum confinement effects arise when the pores become extensive enough to overlap with each other, generating nanometer-scale silicon filaments. As expected from the quantum confinement relationship [18], the red to green color of photoluminescence occurs at energies significantly higher than the bandgap energy of bulk silicon (1.1eV, in the near-infrared). A little after, enormous work focused on creating silicon-based optoelectronic switches, displays, and lasers. At the same time, the unique properties of the material, such as large surface area, controllable pore sizes, convenient surface chemistry, and compatibility with conventional silicon microfabrication technologies, prompted research into novel applications: various biomedical sensors, optics, and electronics applications emerged [19].

This study examines the use of porous silicon with different porosity values as an antireflection coating to reduce light reflection and improve the conversion efficiency of silicon solar cells. Two different cases were considered: single antireflection layer and multilayered stack antireflection coating. The effect of the incidence angle was examined along with the determination of the reflectivity in each case.

II. COMPUTATIONAL METHODOLOGY

The Stratified Medium Theory (SMT) was used for the calculation of the reflectivity of the studied ARCs. This approach is known to combine a simple formalism and great flexibility of use. More insights and details about SMT are given in [20-22]. Within SMT, the inhomogeneous medium is subdivided into N inhomogeneous strata with refractive index $\widetilde{N}_j$. Each stratum is represented by a complex characteristic matrix M_j. Matrices M_0 and M_s correspond to ambient and substrate semi-infinite media, respectively, as detailed in [21,22]. The simplified relation:

$$\begin{bmatrix} a \\ b \end{bmatrix} = M_0\left(\prod_{j=1}^{N} M_j\right)M_s \quad (1)$$

can be written more explicitly:

$$\begin{bmatrix} a \\ b \end{bmatrix} = \begin{bmatrix} p_0^{+1} \\ p_0^{-1} \end{bmatrix} \prod_{j=1}^{N} \begin{bmatrix} \cos\delta_j & p_j^{-1}\sin\delta_j \\ ip_j\sin\delta_j & \cos\delta_j \end{bmatrix} \begin{bmatrix} 1 \\ p_s \end{bmatrix} \quad (2)$$

where δ_j is the phase shift due to the j^{th} stratum:

$$\delta_j = \frac{2\pi}{\lambda}\widetilde{N}_j d_j \cos\theta_j \quad (3)$$

and θ_j is determined from the incidence angle θ_0 according to the Snell-Descartes law:

$$\widetilde{N}_j \sin\theta_j = \widetilde{N}_0 \sin\theta_0 \quad (4)$$

For Transverse Electric (TE) polarization, $p_j = \widetilde{N}_j cos\theta_j$, and for Transverse Magnetic (TM) polarization, $p_j = \widetilde{N}_j / cos\theta_j$. Fresnel coefficients are calculated for both polarizations and each wavelength using:

$$R_{TE} = \left(\frac{a}{b}\right)_{TE}$$

and

$$R_{TM} = \left(\frac{a}{b}\right)_{TM} \quad (5)$$

Reflectivity can then be expressed as [21,22]:

$$R = \frac{1}{2}(R_{TE}R_{TE}^{*} + R_{TM}R_{TM}^{*}) \quad (6)$$

III. RESULTS AND DISCUSSION

A. Single Antireflection Layer

Figure 1 represents the reflectivity as a function of the incident wavelength for a single antireflection layer made of porous silicon with different values of porosity ranging between 55 and 80%. As can be noted, the reflectivity at first increases, reaching a maximum value for wavelengths below 400nm and then decreases until the wavelengths approach 630nm. Beyond 630nm, the reflectivity increases again. Furthermore, the lowest reflectivity is obtained in the vicinity of 630nm and corresponds to porosity values of 55, 60, and 65%. The best-retained result corresponds to a porosity of 60% and therefore to a refractive index of 1.96. This is in agreement with the findings reported in [23]. However, the reflectivity in the vicinity of 630nm in this study is better than the one obtained in [23]. In general, good agreement is recorded for other wavelengths.

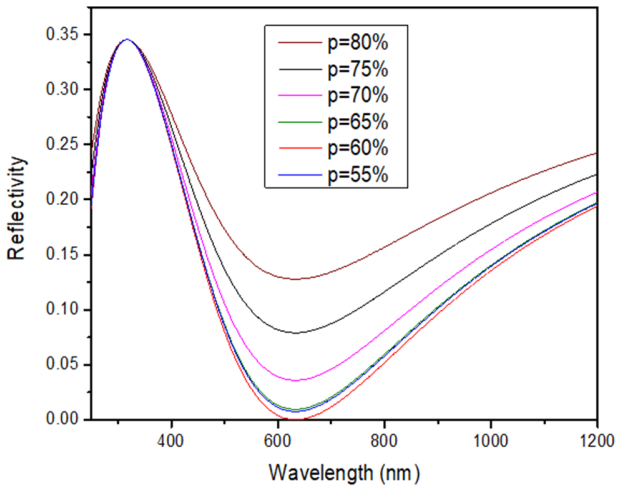

Fig. 1. Reflectivity vs wavelength for a single porous silicon anti-reflection layer for different porosity values.

B. Effect of the Number of Layers in the Stack

The anti-reflective coating is obtained by stacking a certain number of periods, each of them consisting of two layers of porous silicon with different porosity values. The effect of the number of layers of the stack on the reflectivity is illustrated in Figure 2. As can be noted, the stack of layers with minimum reflectivity consists of alternating layers of respective porosities 65/60% with n_L=6 periods. However, the corresponding wavelength range is relatively narrow. The stack with 6 layers

of respective porosity values of 65/55% is preferable as it is characterized by a wider range of wavelengths extending from 580 to 690nm. The corresponding minimum reflectivity is as low as 1.46%. This can be traced back to the effect of the quantum confinement phenomenon. More details about this phenomenon can be found in [24-28]. These results are qualitatively similar in trend to the requirements reported in [29-35].

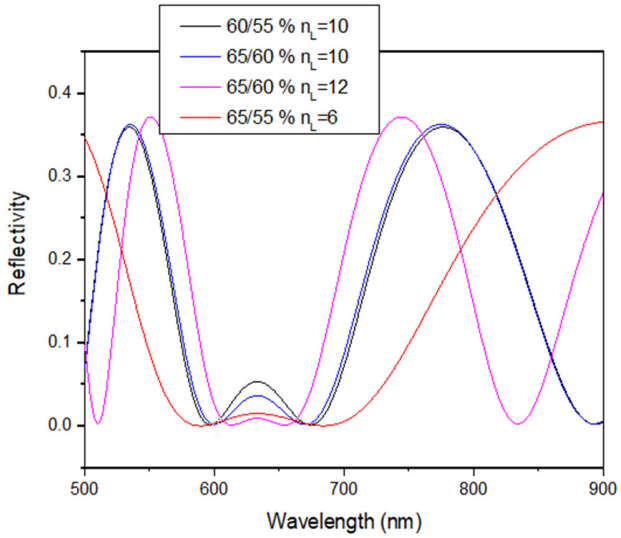

Fig. 2. Reflectivity vs wavelength for a stack of porous silicon anti-reflection coatings for different porosity values.

C. *Effect of the Angle of Incidence for a Single ARL*

The influence of the angle of incidence on the reflectivity of a simple porous silicon antireflection layer of 60% porosity with refractive index 1.96 is shown in Figure 3.

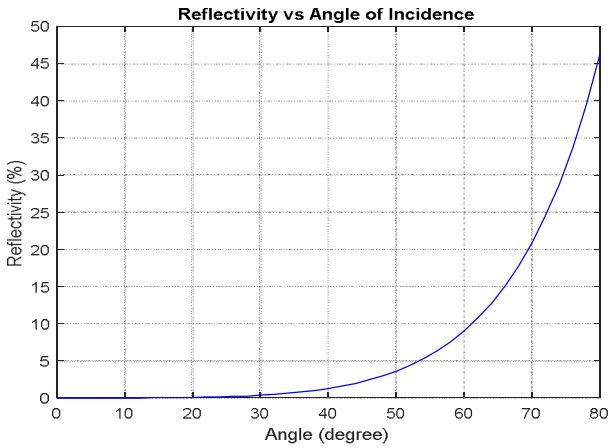

Fig. 3. Reflectivity as a function of the angle of incidence for a single porous silicon anti-reflection coating with a porosity of 60%.

As it can be observed, the reflectivity is almost zero for angles of incidence less than 30°. This reflectivity increases up to 0.05 for angles between 30° and 53°, then it increases more for higher values of the angle of incidence. Therefore, it can be concluded that the angle of incidence affects the reflectivity only slightly until the angle of incidence exceeds 55°. Qualitatively similar behavior was reported in [22].

This result is confirmed in Figure 4 which represents the dependence on the wavelength of the reflectivity of a single layer of porous silicon used as an antireflection coating on a silicon-based photovoltaic cell, for different angles of incidence ranging from 0 to 80°. It is noted that the lowest reflectivity is recorded for normal incidence, and increasing the angles to more than 30° deteriorates the reflectivity.

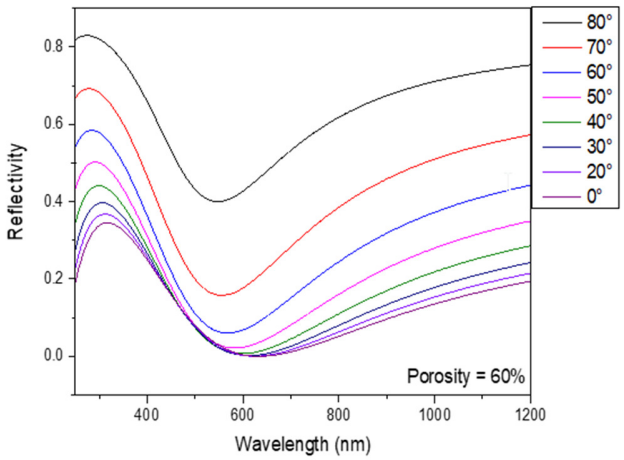

Fig. 4. Reflectivity vs. wavelength for a single porous silicon anti-reflection layer with 60% porosity for different incidence angles.

D. *Effect of the Angle of Incidence for a Stack of Anti-Reflection Layers*

The chosen stack of layers was the optimal one consisting of stacking of porosity 65/55% with 1.78/2.14 refractive indices and n_L=6 (n_L being the number of layers in the stack). The corresponding reflectivity is plotted as a function of the angle of incidence in Figure 5.

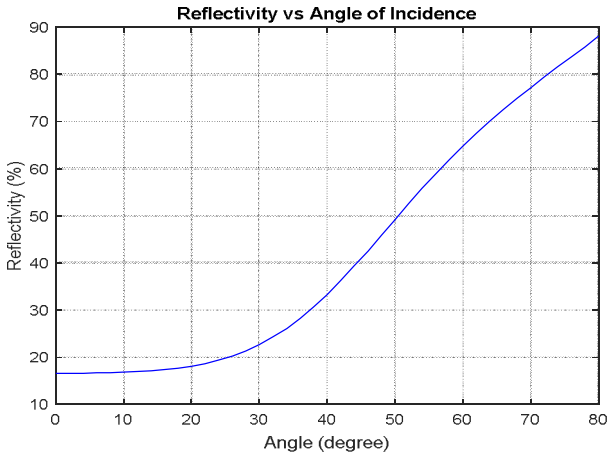

Fig. 5. Reflectivity as a function of the angle of incidence for a stack of porous silicon antireflection layers with a porosity of 65%/55%.

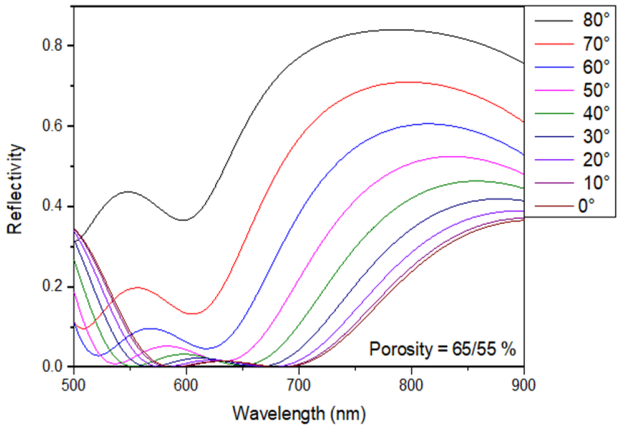

Fig. 6. Reflectivity vs. wavelength for a stack of porous silicon anti-reflection layers with a porosity of 65%/55% for different incidence angles.

As can be observed, the reflectivity is between 1.66% and 18% for angles of incidence less than 20°, and between 18 and 22.7% for angles between 20°-30°, and increases rapidly for angles above 30°. This confirms that the lowest reflectivity corresponds to the normal incidence, while the reflectivity of the stack increases when moving away from normal incidence.

Figure 6 shows the reflectivity as a function of wavelength for angles of incidence ranging from 0 to 80°, for a stack of porous silicon anti-reflection layers with a porosity of 65/55%. It can be noted that the lowest reflectivity is recorded for the case of normal incidence. Furthermore, as the angle of incidence exceeds 20°, the reflectivity increases and shifts towards the lowest wavelengths.

The conversion efficiency of a solar cell can be improved by making a judicious choice of the number of junctions in the cell and the materials whose energy gap can be controlled. This control can be easily obtained by alloying binary compounds to obtain ternary semiconductor alloys such as $GaAs_{1-x}N_x$, $GaSb_{1-x}N_x$, or $InAs_{1-x}N_x$ [36-39]. Other alloys that contain low concentration magnetic elements, called dilute magnetic semiconductors, can also be considered [40-43]. Their gaps are controllable by varying the concentration of the magnetic element and also by taking advantage of the spin channels.

IV. CONCLUSION

The reflectivity of a single antireflective layer made of porous silicon along with that of a multilayered stack of the same material was examined to reduce the reflection losses occurring in silicon solar cells. The effect of porosity, number of layers, and incidence angle was addressed and analyzed. The optimal porosity value was found to be 60% for the single anti-reflective layer and 65/55% for the multilayered antireflective stack with 6 periods. The incidence angle effect was less for the single antireflective layer than for the stack. These results show that porous silicon can be used efficiently as an anti-reflective coating and can lead to improvements in the photovoltaic solar cell conversion efficiency.

REFERENCES

[1] M. Orgeret, *Les piles solaires: le composant et ses applications*. Paris: Masson, 1985.

[2] "SolarPower Europe – Leading the Energy Transition." https://www.solarpowereurope.org/ (accessed Feb. 23, 2022).

[3] "CORDIS | European Commission." https://cordis.europa.eu/ (accessed Feb. 23, 2022).

[4] A. Bouarissa, A. Gueddim, N. Bouarissa, and H. Maghraoui-Meherezi, "Modeling of ZnO/MoS2/CZTS photovoltaic solar cell through window, buffer and absorber layers optimization," *Materials Science and Engineering: B*, vol. 263, Jan. 2021, Art. no. 114816, https://doi.org/10.1016/j.mseb.2020.114816.

[5] A. Hedibi, A. Gueddim, and B. Bentria, "Numerical Modeling and Optimization of ZnO:Al/iZnO/ZnMgO/CZTS Photovoltaic Solar Cell," *Transactions on Electrical and Electronic Materials*, vol. 22, no. 5, pp. 666–672, Jul. 2021, https://doi.org/10.1007/s42341-020-00278-w.

[6] A. Gueddim, N. Bouarissa, A. Naas, F. Daoudi, and N. Messikine, "Characteristics and optimization of ZnO/CdS/CZTS photovoltaicsolar cell," *Applied Physics A*, vol. 124, no. 2, Oct. 2018, Art. no. 199, https://doi.org/10.1007/s00339-018-1626-1.

[7] J. A. Dobrowolski, D. Poitras, P. Ma, H. Vakil, and M. Acree, "Toward perfect antireflection coatings: numerical investigation," *Applied Optics*, vol. 41, no. 16, pp. 3075–3083, Jun. 2002, https://doi.org/10.1364/AO.41.003075.

[8] D. Poitras and J. A. Dobrowolski, "Toward perfect antireflection coatings. 2. Theory," *Applied Optics*, vol. 43, no. 6, pp. 1286–1295, Feb. 2004, https://doi.org/10.1364/AO.43.001286.

[9] E. B. Grann, M. G. Moharam, and D. A. Pommet, "Optimal design for antireflective tapered two-dimensional subwavelength grating structures," *JOSA A*, vol. 12, no. 2, pp. 333–339, Feb. 1995, https://doi.org/10.1364/JOSAA.12.000333.

[10] K. L. Chopra, D. K. Pandya, and L. K. Malhotra, "Solar Selective Coatings," presented at the Third Workshop on Thin Films Physics and Technology, New Delhi, India, Mar. 1999, pp. 231–326.

[11] P. Gupta, V. L. Colvin, and S. M. George, "Hydrogen desorption kinetics from monohydride and dihydride species on silicon surfaces," *Physical Review B*, vol. 37, no. 14, pp. 8234–8243, Feb. 1988, https://doi.org/10.1103/PhysRevB.37.8234.

[12] P. Gupta, A. C. Dillon, A. S. Bracker, and S. M. George, "FTIR studies of H2O and D2O decomposition on porous silicon surfaces," *Surface Science*, vol. 245, no. 3, pp. 360–372, Dec. 1991, https://doi.org/10.1016/0039-6028(91)90038-T.

[13] A. C. Dillon, P. Gupta, M. B. Robinson, A. S. Bracker, and S. M. George, "FTIR studies of water and ammonia decomposition on silicon surfaces," *Journal of Electron Spectroscopy and Related Phenomena*, vol. 54–55, pp. 1085–1095, Jan. 1990, https://doi.org/10.1016/0368-2048(90)80298-O.

[14] A. C. Dillon, M. B. Robinson, M. Y. Han, and S. M. George, "Diethylsilane Decomposition on Silicon Surfaces Studied Using Transmission FTIR Spectroscopy," *Journal of The Electrochemical Society*, vol. 139, no. 2, pp. 537-543, Feb. 1992, https://doi.org/10.1149/1.2069252.

[15] R. C. Anderson, R. S. Muller, and C. W. Tobias, "Investigation of porous silicon for vapor sensing," Lawrence Livermore National Lab. (LLNL), Livermore, CA (United States); Berkeley Sensor and Actuator Center, CA (USA), UCRL-21267, Oct. 1989. https://doi.org/10.2172/5234679.

[16] L. T. Canham, "Silicon quantum wire array fabrication by electrochemical and chemical dissolution of wafers," *Applied Physics Letters*, vol. 57, no. 10, pp. 1046–1048, Jun. 1990, https://doi.org/10.1063/1.103561.

[17] V. Lehmann and U. Gösele, "Porous silicon formation: A quantum wire effect," *Applied Physics Letters*, vol. 58, no. 8, pp. 856–858, Oct. 1991, https://doi.org/10.1063/1.104512.

[18] L. Brus, "Size dependent development of band-structure in semiconductor crystallites," *New Journal of Chemistry*, vol. 11, no. 2, pp. 123–127.

[19] M. J. Sailor, "Sensor applications of porous silicon," in *Properties of Porous Silicon*, London, UK: INSPEC - The Institution of Electrical Engineers, 1997, pp. 364–370.

[20] P. Nubile, "Analytical design of antireflection coatings for silicon photovoltaic devices," *Thin Solid Films*, vol. 342, no. 1, pp. 257–261, Nov. 1999, https://doi.org/10.1016/S0040-6090(98)01446-1.

[21] M. Born and E. Wolf, Principles of Optics: Electromagnetic Theory of Propagation, Interference and Diffraction of Light, 7th ed. Cambridge, UK: Cambridge University Press, 1999.

[22] N. Fakroun, A. Gueddim, D. Guibadj, and N. Bouarissa, "Numerical Study of Zn0.66Mg0.34Se/Zn0.74Cd0.26Se Bragg Reflector: Normal and Oblique Incidence," *Transactions on Electrical and Electronic Materials*, vol. 20, no. 6, pp. 537–541, Sep. 2019, https://doi.org/10.1007/s42341-019-00146-2.

[23] H. Lee, E. Lee, and S. Lee, "Investigation of nano-porous silicon antireflection coatings for crystalline silicon solar cells," in *2006 IEEE Nanotechnology Materials and Devices Conference*, Gyeongju, South Korea, Oct. 2006, vol. 1, pp. 340–341, https://doi.org/10.1109/NMDC.2006.4388757.

[24] D. Rahou, H. Bekhouche, E. A. Ghezal, A. Gueddim, N. Bouarissa, and H. Ziani, "Electronic and optical properties of InSb quantum dots from pseudopotential calculation," *Chinese Journal of Physics*, vol. 66, pp. 206–213, May 2020, https://doi.org/10.1016/j.cjph.2020.05.001.

[25] H. Bekhouche, A. Gueddim, N. Bouarissa, and N. Messikine, "Phonon and Polaron properties in InSb spherical quantum dots," *Chinese Journal of Physics*, vol. 65, pp. 146–152, Mar. 2020, https://doi.org/10.1016/j.cjph.2020.02.017.

[26] H. Bekhouche, D. Rahou, A. Gueddim, M. K. Abdelhafidi, and N. Bouarissa, "Electron states, effective masses and transverse effective charge of InAs quantum dots," *Optical and Quantum Electronics*, vol. 50, no. 8, Apr. 2018, Art. no. 309, https://doi.org/10.1007/s11082-018-1576-z.

[27] A. Gueddim, T. Eloud, N. Messikine, and N. Bouarissa, "Energy levels and optical properties of GaN spherical quantum dots," *Superlattices and Microstructures*, vol. 77, pp. 124–133, Jan. 2015, https://doi.org/10.1016/j.spmi.2014.11.003.

[28] T. Eloud, A. Gueddim, and N. Bouarissa, "Optoelectronic Properties of Nanosized GaAs," *Journal of New Technology and Materials*, vol. 4, no. 1, pp. 116–122, 2014, https://doi.org/10.12816/0010314.

[29] R. Abbassi, A. Boudjemline, A. Abbassi, A. Torchani, H. Gasmi, and T. Guesmi, "A Numerical-Analytical Hybrid Approach for the Identification of SDM Solar Cell Unknown Parameters," *Engineering, Technology & Applied Science Research*, vol. 8, no. 3, pp. 2907–2913, Jun. 2018, https://doi.org/10.48084/etasr.2027.

[30] S. Saad, "Enhancement of Solar Cell Modeling with MPPT Command Practice with an Electronic Edge Filter," *Engineering, Technology & Applied Science Research*, vol. 11, no. 4, pp. 7501–7507, Aug. 2021, https://doi.org/10.48084/etasr.4304.

[31] V. V. Prabhakaran and A. Singh, "Enhancing Power Quality in PV-SOFC Microgrids Using Improved Particle Swarm Optimization," *Engineering, Technology & Applied Science Research*, vol. 9, no. 5, pp. 4616–4622, Oct. 2019, https://doi.org/10.48084/etasr.2963.

[32] A. Bellouche, A. Gueddim, S. Zerroug, and N. Bouarissa, "Elastic properties and optical spectra of ZnS1−xOx dilute semiconductor alloys," *Optik*, vol. 127, no. 23, pp. 11374–11378, Dec. 2016, https://doi.org/10.1016/j.ijleo.2016.09.034.

[33] A. Gueddim, S. Zerroug, N. Bouarissa, and N. Fakroun, "Study of the elastic properties and wave velocities of rocksalt Mg1−xFexO: ab initio calculations," *Chinese Journal of Physics*, vol. 55, no. 4, pp. 1423–1431, May 2017, https://doi.org/10.1016/j.cjph.2017.04.009.

[34] A. Bouarissa, A. Gueddim, N. Bouarissa, and H. Maghraoui-Meherzi, "Optical response and magnetic moment of MoS_2 material," *Optik*, vol. 208, Dec. 2020, Art. no. 164080, https://doi.org/10.1016/j.ijleo.2019.164080.

[35] H. Ziani and A. Gueddim, "Structural, Elastic and Electronic Properties of Transition Metal Hydrides TiH2 and ZrH2 from First Principles Calculations," in *2020 6th International Symposium on New and Renewable Energy (SIENR)*, Ghadaia, Algeria, Jul. 2021, pp. 1–4, https://doi.org/10.1109/SIENR50924.2021.9631902.

[36] A. Gueddim, R. Zerdoum, and N. Bouarissa, "Dependence of electronic properties on nitrogen concentration in GaAs1−xNx dilute alloys," *Journal of Physics and Chemistry of Solids*, vol. 67, no. 8, pp. 1618–1622, May 2006, https://doi.org/10.1016/j.jpcs.2006.02.007.

[37] A. Gueddim, R. Zerdoum, and N. Bouarissa, "Effect of nitrogen concentration on mechanical properties of GaAs1−xNx dilute alloys," *Materials Science and Engineering: B*, vol. 131, no. 1, pp. 111–115, Apr. 2006, https://doi.org/10.1016/j.mseb.2006.03.032.

[38] A. Gueddim, R. Zerdoum, and N. Bouarissa, "Alloy composition and optoelectronic properties of dilute GaSb1−xNx by pseudo-potential calculations," *Physica B: Condensed Matter*, vol. 389, no. 2, pp. 335–342, Oct. 2007, https://doi.org/10.1016/j.physb.2006.07.008.

[39] A. Gueddim and N. Bouarissa, "Electronic structure and optical properties of dilute InAs1-xNx: pseudopotential calculations," *Physica Scripta*, vol. 80, no. 1, Mar. 2009, Art. no. 015701, https://doi.org/10.1088/0031-8949/80/01/015701.

[40] M. Ajmal Khan, A. Gueddim, N. Bouarissa, H. Algarni, and H. Ziani, "Band parameters for $Zn_{1-x}Mo_xTe$ studied by means of spin-polarized first-principles calculations," *Journal of Computational Electronics*, vol. 19, no. 1, pp. 38–46, Nov. 2020, https://doi.org/10.1007/s10825-019-01430-3.

[41] A. Gueddim, M. E. Madjet, S. Zerroug, and N. Bouarissa, "First-principles investigations of electronic properties and optical spectra of $Cd_{1-x}Mn_xTe$ dilute magnetic semiconductors," *Optical and Quantum Electronics*, vol. 48, no. 12, Aug. 2016, Art. no. 551, https://doi.org/10.1007/s11082-016-0818-1.

[42] N. Bouarissa, A. Gueddim, S. A. Siddiqui, M. Boucenna, and A. Al-Hajry, "First-principles study of dielectric properties and optical conductivity of $Cd_{1-x}Mn_xTe$," *Superlattices and Microstructures*, vol. 72, pp. 319–324, May 2014, https://doi.org/10.1016/j.spmi.2014.05.010.

[43] S. Zerroug, A. Gueddim, and N. Bouarissa, "Composition dependence of fundamental properties of $Cd_{1-x}Co_xTe$ magnetic semiconductor alloys," *Journal of Computational Electronics*, vol. 15, no. 2, pp. 473–478, Mar. 2016, https://doi.org/10.1007/s10825-016-0802-9.